Hindawi
Advances in Civil Engineering
Volume 2022, Article ID 5447614, 12 pages
https://doi.org/10.1155/2022/5447614

Research Article

Stability Analysis of Blasting Excavation for High Rock Slope of Highway Reconstruction and Expansion

Ruixin Zhao,[1] **Zhongju Feng**,[1] **Jianwei Huo**,[2] **Guan Jiang**,[1] **and Fuchun Wang**[1]

[1]*School of Highway, Chang'an University, Xi'an, Shaanxi 710064, China*
[2]*China State Construction International Investments Limited, Hangzhou, Zhejiang, 310000, China*

Correspondence should be addressed to Ruixin Zhao; zhaorxin@chd.edu.cn

Received 16 January 2022; Accepted 14 June 2022; Published 31 July 2022

Academic Editor: Rongchao Xu

To analyze the stability of high rock slopes under millisecond blasting in the paper, time-history curves of millisecond blasting dynamic loads are established based on field data from the reconstruction and extension project of the Beijing-Shanghai Highway. Numerical simulations and field monitoring data are used to study the dynamic response characteristics of the slope stress, displacement, velocity, and safety factor at different times. The results show that the local shear stress near the blasting area is greater than the shear strength of the rock mass, which has a good effect on precracking. Additionally, the peak vibration law of the particles near the blasting area is found to change synchronously with the application of the dynamic blast load; as the distance increases, the law gradually weakens and peak vibration occurs only near the maximum value. Moreover, the safety factor of the slope exhibits a decreasing periodic variation. When the dynamic blast load F reaches the maximum load F_{max} and 0.6 F_{max}, the corresponding safety factor reaches the minimum load.

1. Introduction

With the increasing traffic flow in China, the existing highway lanes difficultly meet the actual societal needs, and the number of highway reconstruction and expansion projects is sharply increasing [1–4]. Consequently, the stability problems of the secondary excavation of existing slopes during the reconstruction and expansion process have become popular research topics. The reconstruction and extension construction without traffic interruption is a big feature of expressway reconstruction and extension projects. In order to speed up the construction progress, blasting excavation has become an important means of slope excavation.

The determination of blasting dynamic load is the key to the research. Henrych and Chen [5, 6] believed that the blasting dynamic load was a triangular pulse function and set the blasting time to 7 ms. They considered a linear change with a shorter rise time and a longer fall time. Sitnikova [7] believed that the blasting dynamic load first increased linearly within a period of time and then began to decay exponentially. Aksoylar and Balkan [8, 9] believed that the blasting dynamic load was a changing nonlinear function relationship. Jiang [10] simulated the change of blasting dynamic load by changing the stress-strain relationship. Liu and Wang proposed effective models for calculation of the equivalent uniform blast load for non-uniform blast load using the equivalent single-degree-of-freedom (SDOF) approach [11, 12].

After determining the blasting dynamic load, the study of blasting stability has become the focus of research. Dowding and Zhang [13, 14] used numerical simulation software to study the energy distribution characteristics and waveform response characteristics of each frequency band of the slope under blast loads. Kesimal [15] studied the effect of blast acceleration on slope shear failure via on-site blast monitoring, laboratory test evaluations, and the limit equilibrium method and considered that uncontrolled blast acceleration and heavy rainfall have greater impacts on slope shear failure. Hu and Ren [16, 17] used ANSYS software to study the dynamic response characteristics of the secondary excavation of slopes under blast loads and predicted the entire process of slope damage.

Some scholars have also studied millisecond blasting. Millisecond blasting is a blasting method in which blasts are made in a certain order at a time interval of milliseconds

between blastholes and rows or within blastholes [18, 19]. Blair [20–23] studied the vibration effect of millisecond blasting, based on which a nonlinear superposition model of single-hole blasting and a linear superposition model of porous microblasting were proposed via the analysis of experimental data. Chen and Liu [24, 25] analyzed the effect of the millisecond blasting of a cylindrical charge structure on the slope vibration effect via vibration velocity waveform function prediction. Mandal [26] studied the calculation method of the vibration velocities of different measurement points under the condition of a single-hole cylindrical charge with a millisecond blasting time interval of 1 ms. Kalinski [27] used numerical simulation to study the effects of the hole distance, blasting direction, and millisecond blasting time interval on the vibration effect of porous millisecond blasting. Yang [28] studied the main crack propagation characteristics of millisecond blasting under respective time-delay conditions of 20 μs and 40 μs and compared the differences in the shape and process of the failures of the specimen under the two conditions.

Based on the blasting project on the left side of section K551 + 714~K552 + 116 of the reconstruction project of the Beijing-Shanghai Expressway, numerical simulation software was utilized in the present study to establish a dynamic load time-history curve between blastholes under differential blasting. The mechanism of millisecond blasting is proven via the slope shear stress, displacement, and velocity of different measurement points, and the distribution law of the safety factor.

2. The Blasting Engineering

2.1. Engineering Background. The slope was originally constructed by mechanical crushing, and the remaining first-grade platform and some second-grade platform were not excavated. Millisecond blasting was employed to speed up the progress of the project. The dotted lines in Figure 1 indicate the blasting area; its east-west length is 300 m, the subgrade is 15 m wide from north to south, the top of the blasting step is 14 m, the average height is 9 m, and the slope height is 39.7 m. The main lithologies of the slope are strongly and moderately weathered limestone as shown in Figure 2.

2.2. Blasting Parameters. The parameters of this blasting are selected as shown in Table 1. The layouts of the blasthole charge and the blasthole depth are, respectively, illustrated in Figures 3 and 4.

3. Numerical Simulation

3.1. Determination of Equivalent Dynamic Blast Load. Determining a reasonable dynamic blast load is the key to the accurate calculation of numerical simulation, but there exists no systematic and perfect theoretical method by which the dynamic blast load could be determined at present. In this paper, via the use of the stress time-history analysis, the dynamic blast load is considered to be equivalent to a uniformly distributed concentrated force acting on the

Figure 1: Schematic diagram of the explosion area.

normal direction of the blasthole wall. Because the blasthole diameter is greater than the charge diameter, it is an uncoupled charge. According to the Chapman-Jouguet theory of the detonation waves of condensed explosives [29], the calculation formula of the blasthole wall pressure P_b is modified by

$$P_b = \frac{\rho_0 D^2}{2(k+1)}\left(\frac{d_e}{d_h}\right)^{2k}, \tag{1}$$

where P_b is the blasthole wall pressure (Pa), ρ_0 is the explosive density and is equal to 1300 kg/m^3, $D$is the blasting velocity and is equal to 3600 m/s, k is the isentropic index and is equal to 3, d_e is the charge diameter and is equal to 70 mm, and d_h is the blasthole diameter and is equal to 90 mm.

The time-history curve of the equivalent dynamic blast load is determined according to (2) proposed by National Highway Institute in the United States [30], and other parameters are calculated according to the work by Zou [31].

$$P(t) = 4P_{\mathrm{b}} \times \left[\exp\left(\frac{-B \times t}{\sqrt{2}}\right) - \exp\left(-\sqrt{2}\, B \times t\right)\right], \tag{2}$$

$$B = -\frac{\sqrt{2}\ln(1/2)}{T_r}, \tag{3}$$

$$T_r = \frac{L_1}{D}, \tag{4}$$

where $P(t)$ is the equivalent dynamic blast load (Pa), B is the blast load constant, T_r is the rising time of the dynamic blast load (ms), and L_1 is the charge length and is equal to 7.5 m.

The following values are yielded after calculation: $P_b = 466.2$ MPa, $B = 470$, and $T_r = 2.083 \times 10^{-3} s$.

During numerical simulation modeling, the applied dynamic blast load is converted to the nodal force acting on the element, which is calculated by

$$F = P(t) \times d_{\mathrm{h}} \times r, \tag{5}$$

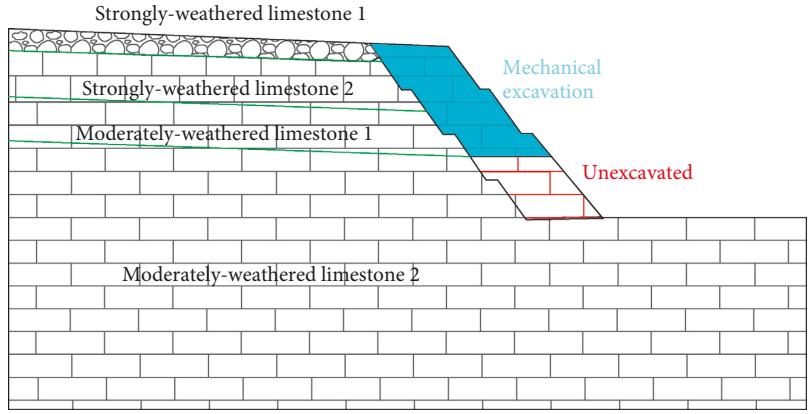

Figure 2: Section locations of the blasting area.

Table 1: Parameters of this blasting.

Parameter	Value
Blasthole diameter (d)	90 mm
Blasthole step height (H)	12 m
Beyond the depth (Δh)	1 m
Blasthole depth (L)	13 m
Chassis resistance line (w)	2.07 ~ 3.09 m
Blasthole density factor (m)	1 m
Blasthole distance (a)	4 m
Row spacing (b)	3.5 m
Unit explosive consumption (q)	0.2 kg/m^3
Tamping length (l)	4.5 m
Maximum explosive charge (Q_{max})	38 kg

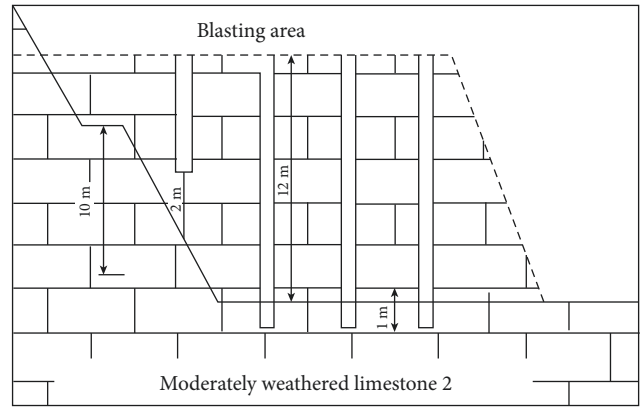

Figure 4: The layout of the blasthole depth.

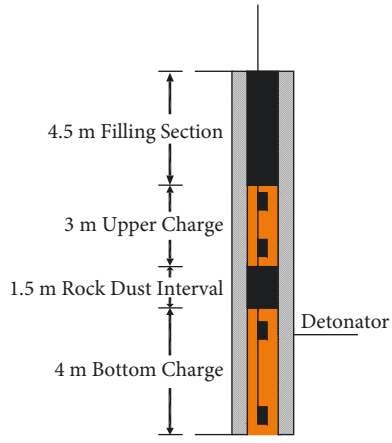

Figure 3: The layout of the blasthole charge.

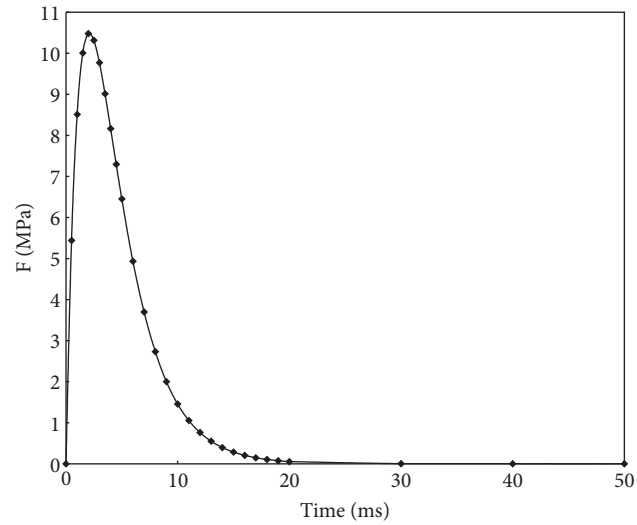

Figure 5: Equivalent dynamic blast load time-history curve.

where r is the distance between two vertical nodes of the blasthole in the model and is equal to 1 m and F is the dynamic blast load applied to the actual model (MPa).

Figure 5 presents the equivalent dynamic blast load time-history curve when the blasting time is set as 50 ms, the influence of the blasthole distance is a, and the proportionality factor is set to $1/a$ during modeling.

By derivation of (5), the corresponding time at the peak value is determined to be $t = 2.086 \times 10^{-3} s$, which is consistent with the calculation in (4). By substituting it back into (5), the corresponding maximum dynamic load is determined to be $F(2.086 \times 10^{-3}) = 10.33$ Mpa.

According to the situation of the site, the connection mode between blastholes is an Ms-4 connection. According to State Administration of Work Safety [32], the time interval of the

Ms-4 connection is 75 ms (+15, −10). Because the load is converted into a nodal dynamic force and acts on the wall of the blasthole, it is considered that the interior of the blasthole is simultaneously blasted, and the time interval between blastholes was set to 75 ms in the numerical simulation calculation, that is, 75 ms for the 1st blasted, 150 ms for the 2nd blasted, 225 ms for the 3rd blasted, and 300 ms for the 4th blasted.

3.2. Mechanical Parameters and Boundary Conditions. The surrounding rock was calculated by the Drucker-Prager yield criterion [33]. This strength theory reflects the influences of volumetric stress, shear stress, and intermediate principal stress on the rock strength and can reflect the reality better than other strength theories. The assumptions obtained by this model are sufficiently reliable for general nonlinear geotechnical analysis, so they are widely used to simulate geotechnical materials. According to the geological prospecting data, the rock mass in the blasting area is divided into four parts, and the material mechanical parameters of the calculation model are reported in Table 2.

When performing dynamic blast analysis, the influence of the reflected stress wave on the boundary surface must be considered. In this work, the viscous boundary condition proposed by Lysmer and Wass is used to absorb the incident wave on the boundary and to reduce its influence on the numerical simulation results [34].

3.3. Model Building. The left slope of section K551 + 714-K552 + 116 was considered as a prototype, and a row of blastholes was selected for research. MIDAS-GTS software was used to build the 2D model. The slope rate was 1 : 0.75, the slope height was 39.7 m, the step height was 10 m, the platform width was 2 m, the total model length was 176 m, the height was 82.7 m, the slope to the right boundary was 60.6 m, and the top of the slope to the left boundary was 80.2 m. The model grid was divided into 4197 units, as presented in Figure 6, and the corresponding stratum distribution map is exhibited in Figure 7.

4. Analysis of Calculation Results

In software, the nonlinear time-history + SRM module is a nonlinear dynamic analysis. The stress state of the rock and soil corresponding to this time point can be obtained by inputting the time in the nonlinear time-history analysis. This numerical simulation mainly studies the stability of the blasting area and its surrounding environment and investigates the stress field, displacement field, and velocity field at different positions in the blasting area and the safety factor of the slope at different times. The specific analysis is as follows.

4.1. Stress Field Analysis at Different Blasting Periods. It can be seen from Figure 8 that after the first to fourth blastholes were blasted, a large shear stress appeared on the first-grade slope, and the maximum values were 1.54 MPa, 3.11 MPa, 3.25 MPa, and 2.05 MPa, respectively. Throughout the blasting process, due to the blast load, a concentrated area of shear stress appeared in the first-grade slope, which is in line with the actual situation. Moreover, a phenomenon of shear stress concentration on the second- and third-grade slopes also occurred. At this time, the shear stresses were 1.24 MPa and 0.58 MPa, respectively; while these did not cause slope instability in the model, attention should be paid to these slopes during actual construction.

Based on the preceding analysis, and according to the stress variation trend, the shear stress nephograms of the slope at each time point within 75 ms after the third blasthole was blasted are presented in Figure 9.

It can be seen from Figure 9 that, during the blasting period of the third blasthole, the stress range of the slope gradually expanded, and the maximum shear stress first increased and then decreased. At 170 ms, near the blasting area, the shear stress reached the peak value of 4.21 MPa, which is slightly larger than the shear strength of the rock mass. This demonstrates that the rock mass in the blasting area experienced local shear failure, and a good precracking effect was obtained during the blasting process of the slope. With the gradual diffusion of the stress field, the shear stress at the toes of the second-grade and third-grade slopes increased slightly, reaching respective maximum values of 2.11 MPa and 1.90 MPa at 200 ms, while the shear stress change of the fourth-grade slope was small with a value of approximately 0.17 MPa.

During the entire blasting process, the four blastholes were blasted in sequence, and the shear stress first increased and then decreased due to the influence of the distance. The former blasthole caused local cracks to form in the rock mass, thereby creating a precracking condition for the later blasthole, and the generation of local cracks slowed the diffusion of stress in the rock mass and promoted the accumulation and superposition of stress. The existence of local cracks will also make the stress waves refract and reflect at the cracks, reduce the disturbance of the load, and play a good role in shock absorption, which is beneficial to the later excavation of the slope.

4.2. Analysis of Displacement Field in Different Time Periods. It can be seen from Figure 10 that after the first blasthole was blasted at 75 ms, the maximum displacement at the top of the first-grade slope was 3.59 mm, and there was no obvious displacement change at other positions. Thereafter, the range of the plastic area of the slope continued to expand. After the third blasthole was blasted at 225 ms, the displacement value at the top of the first-grade slope was 12.55 mm, and the second-, third-, and fourth-grade slopes began to show significant displacement changes with values of 2.92 mm, 2.77 mm, and 2.52 mm, respectively. After the fourth blasthole was blasted, due to its small length, the charge was reduced as compared to the previous three holes, which led to the slower expansion of the plastic zone. At 300 ms, the displacement at the top of the first-grade slope was 16.25 mm, and the displacements at the top of the second-, third-, and fourth-grade slopes were 4.13 mm, 3.89 mm, and 3.85 mm, respectively.

Table 2: Mechanical parameters of materials in the blasting excavation area.

Weathering degree of rock	Elastic modulus (GPa)	Poisson's ratio	Cohesion (kPa)	Internal friction angle φ (°)	Shear strength (MPa)	Compressive strength(MPa)
Strongly weathered limestone 1	5	0.2	20	29	2.7	26.3
Strongly weathered limestone 2	10	0.2	21	33	3.0	29.5
Moderately weathered limestone 1	20	0.2	24	51	3.3	31.2
Moderately weathered limestone 2	25	0.2	26	45	3.9	38.4

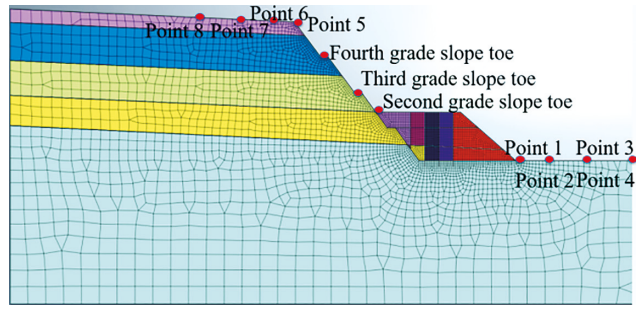

Figure 6: Calculation model diagram.

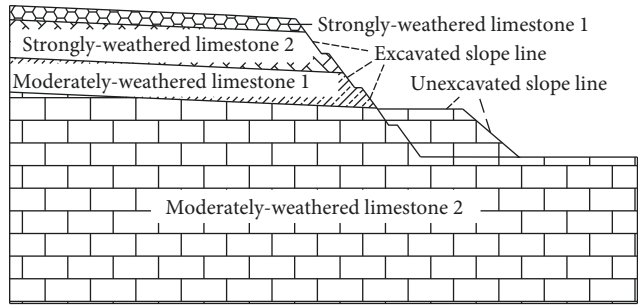

Figure 7: Slope profile.

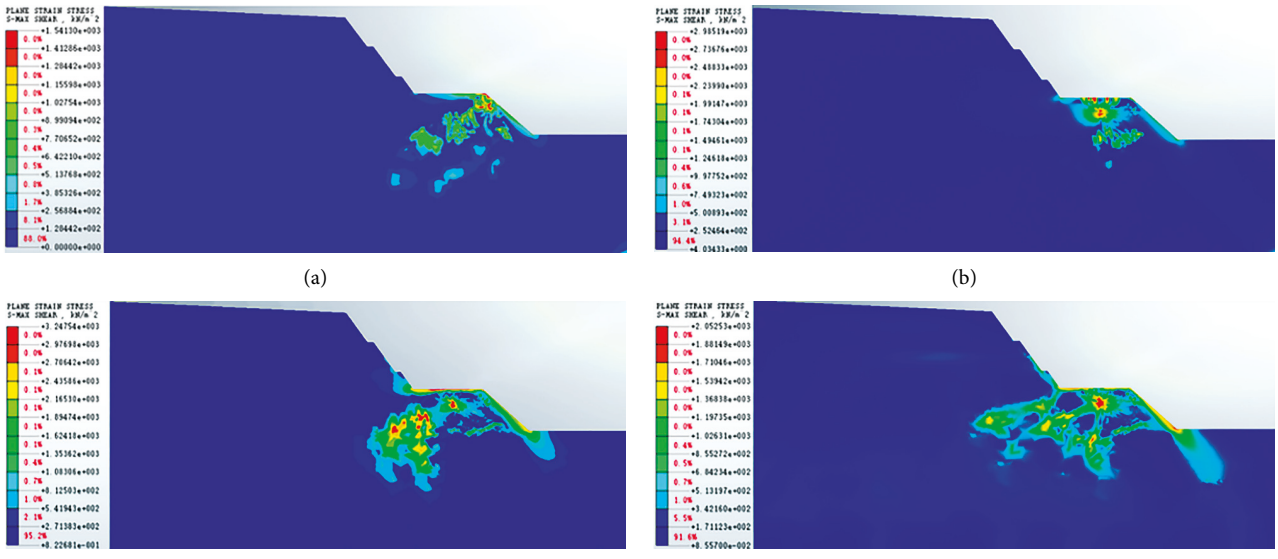

(a) (b) (c) (d)

Figure 8: Slope stress field nephogram at different blasting periods. (a) 75 ms. (b) 150 ms. (c) 225 ms. (d) 300 ms.

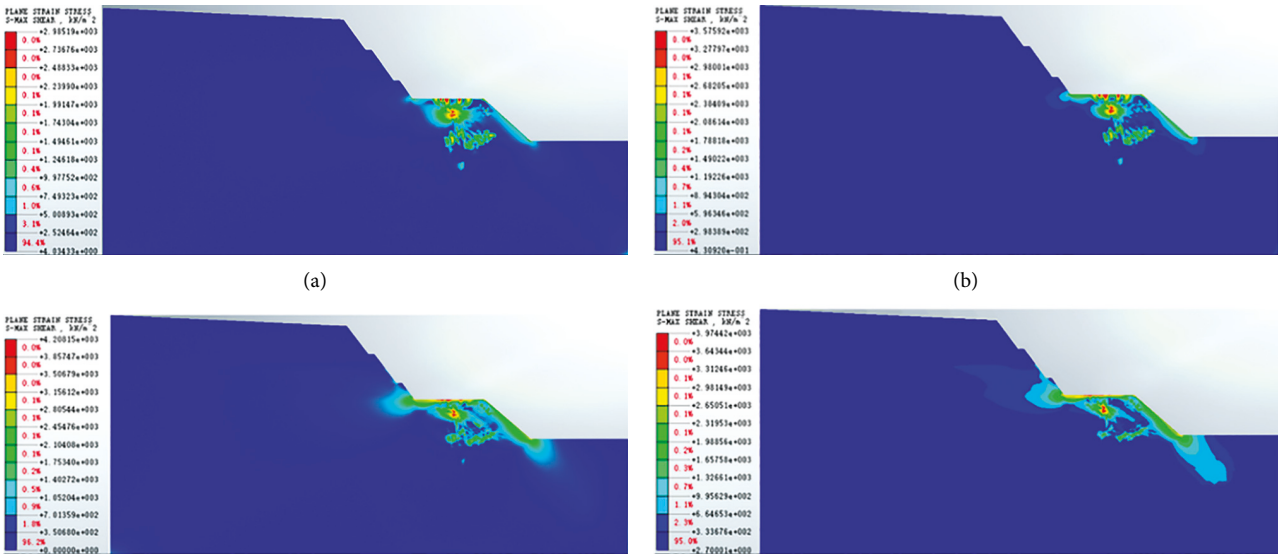

(a) (b) (c) (d)

Figure 9: Stress nephogram after the third blasthole detonation. (a) 150 ms. (b) 155 ms. (c) 170 ms. (d) 200 ms.

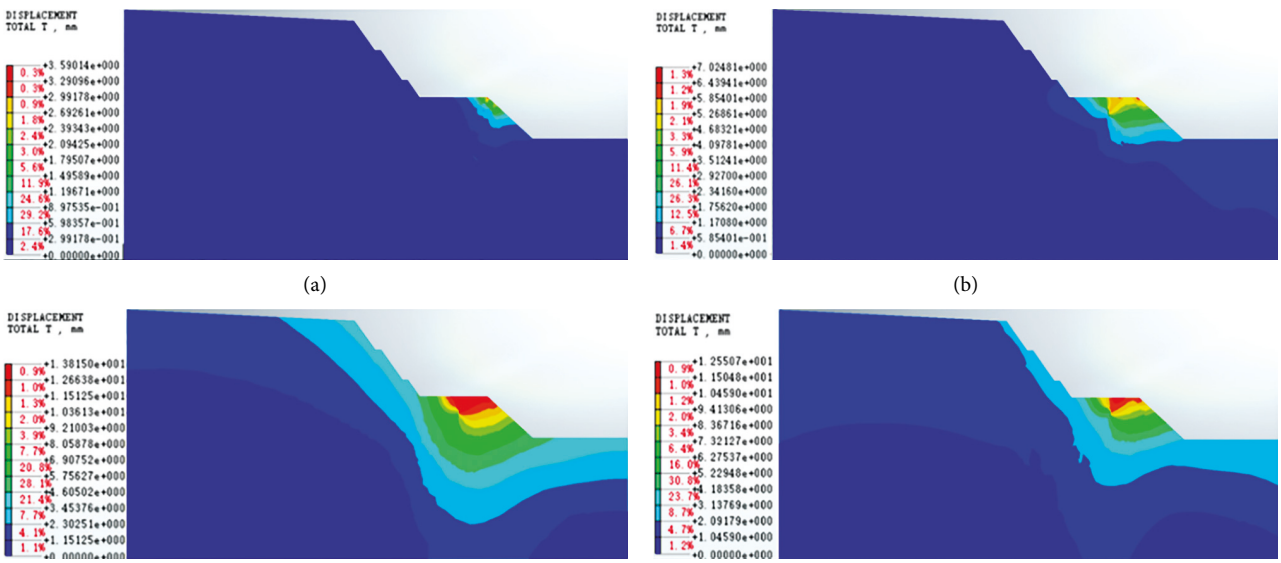

(a) (b) (c) (d)

Figure 10: Displacement field nephograms of different blasting periods. (a) 75 ms. (b) 150 ms. (c) 225 ms. (d) 300 ms.

To study the regional stability of the millisecond blasting of the slope, the displacement nephograms within 75 ms after the fourth blasthole was blasted are shown in Figure 11.

It can be seen from Figure 11 that, during the period when the fourth blasthole was blasted, the overall displacement increment of the slope first increased and then decreased. At 255 ms, the maximum displacement was 19.27 mm at the top of the unexcavated slope, and the displacements at the tops of the second-, third-, and fourth-grade slopes were 5.88 mm, 5.44 mm, and 4.91 mm, respectively. After that, the displacement increment gradually decreased due to the disturbance of the rock mass and the decrease of the blast load. Before and after construction, four measurement points were arranged at the top of the slope, the third platform, and the secondary platform, and the layout of the measurement points is depicted in Figure 12. The displacement changes of each measurement point before and after blasting are reported in Table 3.

According to the on-site measurement data as shown in Table 3, it can be judged that the measured slope displacement before and after blasting was smaller than that of each point during the blasting process. This is because the

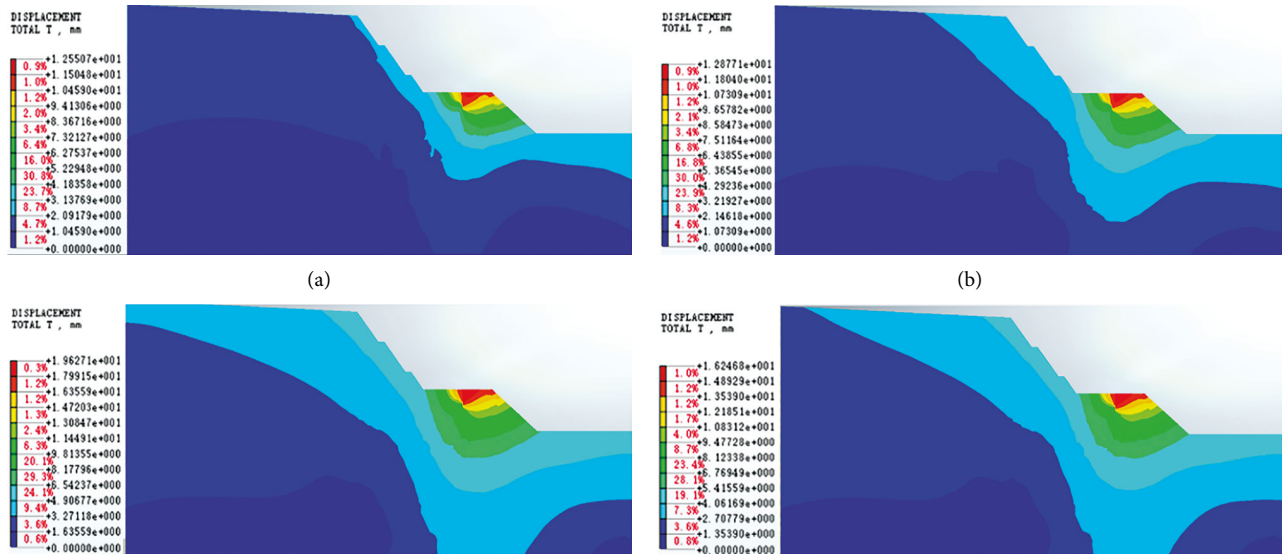

Figure 11: Time-displacement nephograms after the detonation of the fourth blasthole. (a) 225 ms. (b) 240 ms. (c) 255 ms. (d) 275 ms.

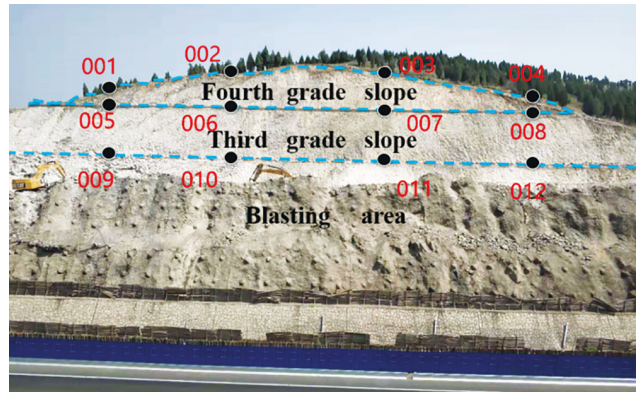

Figure 12: Displacement measurement point layout.

Table 3: Accumulated displacement change before and after blasting (unit: mm).

Position	Top of the slope				Third-grade platform				Second-grade platform			
Point number	01	02	03	04	05	06	07	08	09	10	11	12
Before blasting	11.2	10.0	10.3	10.6	10.8	10.5	11.1	11.1	4.1	3.2	3.0	4.1
After blasting	12.3	10.9	11.2	11.8	12.3	12.1	12.7	12.5	5.8	5.1	4.9	5.8
Displacement difference	1.1	0.9	0.9	1.2	1.5	1.6	1.6	1.4	1.7	1.9	1.9	1.7
Average value	1.025				1.525				1.8			

dynamic blast load disappeared, the stress in the rock was redistributed, and the slope gradually tended to be stable. The average displacement of each measuring point of the secondary platform, tertiary platform, and slope top is 1.8 mm, 1.525 mm, and 1.025 mm, and the displacement value decreases step by step, which is similar to the result of numerical simulation. This demonstrates that there is a collision process between two adjacent blastholes in the process of crushing during millisecond blasting, which makes the distance between the crushed rock and soil relatively close and plays a weak precracking role but does not produce a large slip.

4.3. Velocity Field Analysis at Different Periods. Figures 13(a)–13(c) present the time-history curves of vibration velocity at different measurement points of the slope. Due to the short distance from the slope, the change of the vibration velocity at each measurement point of the slope foot exhibited obvious synchronization with the load time-

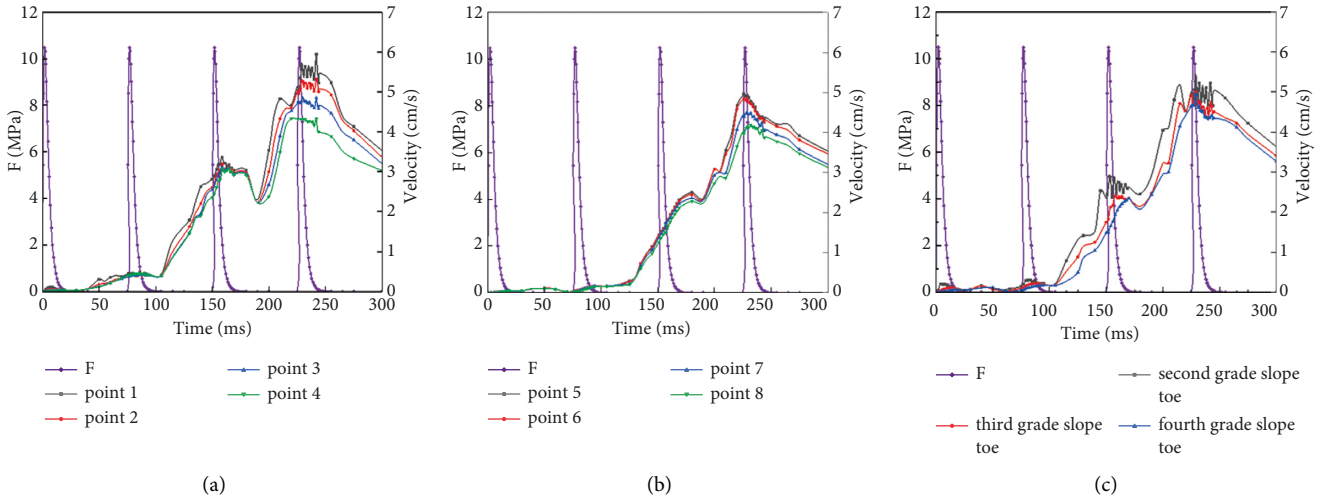

Figure 13: Time-history curves of vibration velocity at different measurement points at different positions and different times during millisecond blasting. (a) On the slope toe. (b) On the slope top. (c) On the slope surface.

history curve. Additionally, in each time period after the dynamic blast load was applied, obvious fluctuation peaks appeared. With the increase of the distance, due to the lag effect of the blast load, the vibration velocity at the four measurement points at the top of the slope started to increase sharply at 130 ms, and peak fluctuations occurred only after the fourth blasthole was blasted. The change rule at the toe of the second-, third-, and fourth-grade slopes is between those at the top and bottom of the slope. The peak vibration velocity of each measurement point decreased with the increase of the distance from the center of the explosion. The peak velocity of the slope foot was the largest, that of the slope surface was the second largest, and that of the slope top was the smallest, which is consistent with the actual situation.

In addition, the maximum peak velocity at 80 m at the top of the slope was 1.8 cm/s, which is less than the safe peak value of 2.5 cm/s specified in the Blasting Safety Regulations, indicating that the use of millisecond blasting has a lesser impact outside the blasting area and meets the safety requirements. According to Huang [35], the velocity of each measurement point was less than 26 cm/s. Tensile cracks may appear locally on the slope rock mass, but these do not pose a hazard to the safety of the slope. According to the on-site investigation, there were local tension cracks on the first-grade slope (as depicted in Figure 14), but no obvious displacement changes occurred, which is in line with the actual on-site construction situation.

4.4. Analysis of Safety Factors in Different Time Periods. Before blasting, the static SRM method was used to analyze the safety factor. The nonlinear time-history added SRM method was then used to analyze the safety factors at each time point of slope blasting excavation. Figures 15 and 16 present the changes in the safety factor at different points in time.

It can be seen from Figures 15 and 16 that the change laws of the safety factor curves for the four blasting operations are consistent. Under the action of the dynamic blast load, the slope safety factor exhibited the following trend: decreasing, increasing, decreasing, increasing, and stabilizing. After half of the mechanical excavation of the slope, the safety factor calculated by static SRM was 2.206. Within 0–2 ms of the dynamic blast load, the original stress balance of the slope was destroyed by the shock wave of the dynamic blast load that was applied instantaneously, causing disturbances in the slope and resulting in the sudden decrease of the slope safety factor. The dynamic blast load at 2 ms reached the maximum, and the safety factor of the slope was reduced to the lowest value, about 1.076. At 2–5 ms, due to the decrease of the dynamic blast load and the short application time, the cumulative effect of the load was not obvious, and the safety factor slightly increased. At 5 ms, the dynamic blast load decreased to 0.6 F_{max}, and the corresponding safety factor increased to 1.098. At 5–10 ms, the dynamic blast load was still reduced, but due to the long period of load application, a significant cumulative effect occurred, resulting in the decrease of the safety factor of the slope. At 10 ms, the dynamic blast load decreased to 0.1 F_{max}, corresponding to the decrease of the safety factor to 1.082, which was still greater than the safety factor corresponding to F_{max}. At 10–20 ms, due to the obvious decrease of the load, the cumulative effect became weaker, resulting in the gradual increase of the slope safety factor. At 20 ms, the dynamic blast load tended to 0, corresponding to the increase of the safety factor to 1.100. At 20–75 ms, because the first blasthole was completed and the second blasthole had not yet been blasted, the cumulative load effect gradually dissipated, and the safety factor of the slope gradually stabilized. The corresponding safety factor was 1.117 at 75 ms.

During the subsequent blasting of the second to fourth blastholes, the safety factor gradually decreased and the change law was similar to that of the blasting of the first blasthole. After the fourth blasthole was blasted, the minimum safety factor was 1.063, and the slope was in a

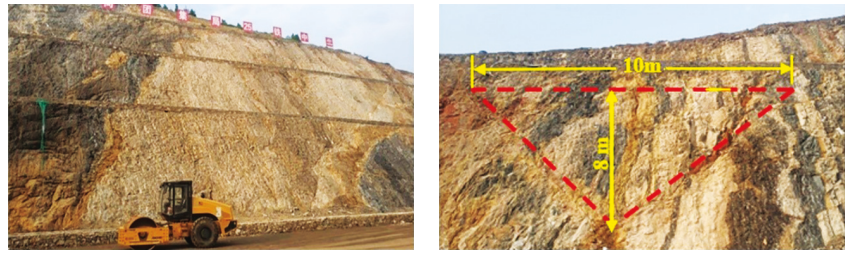

(a) (b)

Figure 14: Site diagrams before and after construction. (a) Schematic diagram. (b) Wedge unstable block.

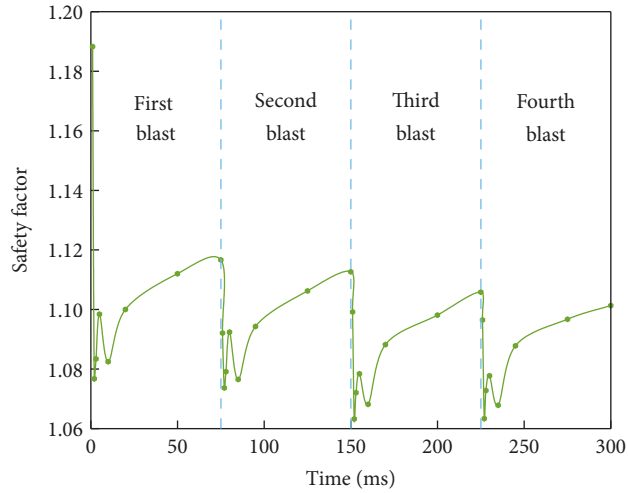

Figure 15: Change of the safety factor of the entire process of millisecond blasting.

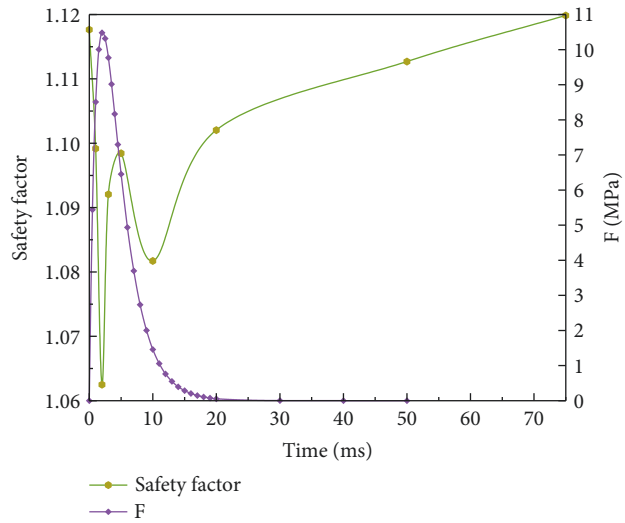

Figure 16: Change of the safety factor during a single equivalent dynamic blast load F.

stable state. This demonstrates that a good blasting effect of the slope was achieved via the use of millisecond blasting, and its stability was within a safe range. However, due to the small safety factor, it is recommended to add necessary support measures during blasting construction to improve the stability of the slope.

To better reflect the advantages of millisecond blasting and explore its mechanism, the simultaneous blasting method was employed and the time-history curves of vibration velocity at the same measurement points and the safety factors at different points in the slope were determined, as presented in Figures 17 and 18.

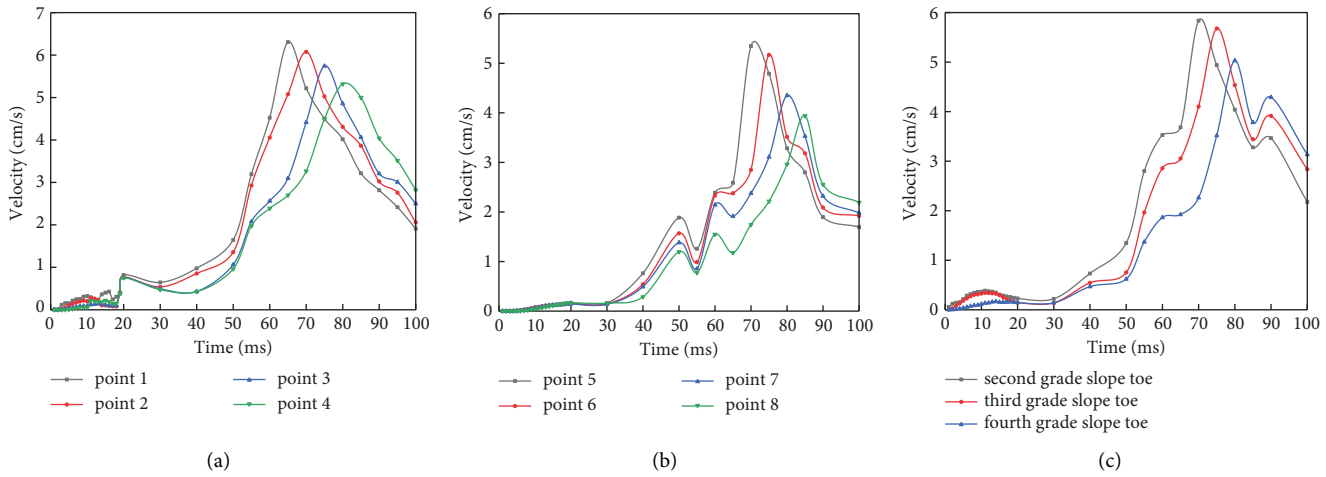

Figure 17: Time-history curve of the vibration velocity of different measurement points at different positions and different times during simultaneous detonation. (a) On the slope toe. (b) On the slope top. (c) On the slope surface.

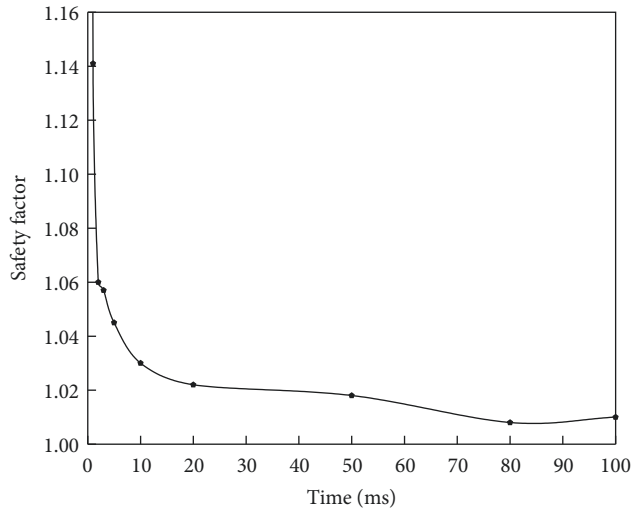

Figure 18: Curve of the safety factor during the entire process of simultaneous detonation.

Because the duration of the blasting of one blasthole via millisecond blasting is 75 ms, the vibration velocity time-history curve of each measurement point of the slope within 100 ms was selected for research. It can be seen from Figures 17(a)–17(c) that the peaks of the vibration velocity of different measurement points for simultaneous blasting are larger than those for millisecond blasting. Additionally, the peaks between the measurement points exhibit a declining and lagging phenomenon, which is similar to the change of the vibration velocity of different measurement points under dynamic blast loads studied by Jiang [36]. It can be seen from Figure 18 that, with the increase of time, the safety factor of simultaneous initiation of the slope gradually decreases, and at the same time point, the safety factor of simultaneous blasting is smaller than that of millisecond blasting, and the stability of the slope is lower. On the one hand, the use of millisecond blasting can reduce the vibration velocity of the rock mass inside the slope, reduce its disturbance, and play a certain role in reducing vibration. On the other hand, due to the obvious resonance phenomenon between the measurement points, when the rock masses in the blasting area collide with each other after weak loosening due to millisecond blasting, the internal energy of the blasting is reduced, which has a good loosening effect.

5. Conclusion

(1) The blasting load constant B was calculated by the equivalent dynamic blast load, which can effectively simulate the blast load time-history curve.

(2) The displacement and maximum shear stress in the blasting zone present the trend from increase to decrease under dynamic blast load. The maximum displacement was 19.27 mm, which indicates that millisecond blasting does few impacts to the stability of the slope. The maximum shear stress was 4.21 MPa, which slightly exceeds the compressive strength of the rock mass. The local rock mass in the blasting area experienced shear failure, which caused weak loosening effect.

(3) Compared with simultaneous blasting, the peak vibration velocity of millisecond blasting is lower, and its resonance effect causes adjacent fragmented rock masses to collide with each other on the slope; this makes them rupture uniformly, reduces the displacement and velocity, and improves the blasting efficiency and energy utilization rate, thereby reducing slope disturbance and playing a good role in reducing vibration.

(4) The safety factor of high rock slopes periodically changes with the application of the millisecond blasting load, and the variation range is 1.06–1.11. When the dynamic blast load F reaches the maximum value (F_{max}), the corresponding safety factor is reduced to the minimum. When $F = 0.6\ F_{max}$, the slope begins to be affected by the obvious cumulative load effect and the safety factor decreases. Until

$F = 0.1\ F_{max}$, the cumulative effect of the load is slowed, the effect on the slope is small, and the safety factor begins to increase and gradually stabilizes. During the construction of the blasting project, these three time points should be considered.

Data Availability

The data used to support the findings of this study are available from the corresponding author upon request.

Conflicts of Interest

The authors declare no conflicts of interest.

Acknowledgments

This research was supported by the National Key R&D Program of China (2018YFC1504801) and the National Natural Science Foundation of China (no. 41907236).

References

[1] L. Chen, J. Chen, and Y. Luo, "Propagation laws of blasting seismic waves in weak rock mass: a case study of muzhailing tunnel," *Advances in Civil Engineering*, vol. 2020, no. 9, 15 pages, Article ID 8818442, 2020.

[2] Y. X. Dong, Z. J. Feng, and J. B. He, "Seismic response of a bridge pile foundation during a shaking table test," *Shock and Vibration*, vol. 2019, Article ID 9726013, 16 pages, 2019.

[3] Z. J. Feng, H. B. Hu, and F. C. Wang, "Field simulation test of bridge pile foundation damage in high altitude and strong salt marsh area," *Journal of Traffic and Transportation Engineering*, vol. 19, no. 3, pp. 46–57, 2019.

[4] R. Macciotta, C. Grpel, and T. Keegan, "Quantitative risk assessment of rock slope instabilities that threaten a highway near canmore, AB, Canada: managing risk calculation uncertainty in practice," *Canadian Geotechnical Journal*, vol. 57, 2019.

[5] J. Abrahamson and G. R. Abrahamson, "The dynamics of explosion and its use," *Journal of Applied Mechanics*, vol. 47, no. 1, p. 2181980.

[6] S. G. Chen, J. Zhao, and Y. X. Zhou, "UDEC modeling of a field explosion test," *International Journal of Blasting and Fragmentation*, vol. 4, pp. 149–163, 2000.

[7] E. Sitnikova, Z. W. Guan, and G. K. Schleyer, "Modelling of perforation failure in fibre metal laminates subjected to high impulsive blast loading," *International Journal of Solids and Structures*, vol. 51, no. 18, pp. 3135–3146, 2014.

[8] C. Aksoylar, A. Omercikoglu, and Z. Mecitoglu, "Nonlinear transient analysis of FGM and FML plates under blast loads by experimental and mixed FE methods," *Composite Structures*, vol. 94, no. 12, pp. 731–744, 2012.

[9] D. Balkan and Z. Mecitoğlu, "Nonlinear dynamic behavior of viscoelastic sandwich composite plates under non-uniform blast load: theory and experiment," *International Journal of Impact Engineering*, vol. 72, no. 11, pp. 85–104, 2014.

[10] Y. Jiang, B. Zhang, and J. Wei, "Study on the dynamic response of polyurea coated steel tank subjected to blast loadings," *Journal of Loss Prevention in the Process Industries*, vol. 67, no. 1, pp. 104–234, 2020.

[11] Y. Liu, J. Yan, and Z. Li, "Improved SDOF and numerical approach to study the dynamic response of reinforced concrete columns subjected to close-in blast loading," *Structures*, vol. 22, no. 1, pp. 341–365, 2020.

[12] W. Wang, D. Zhang, and F. Lu, "A new non-uniform blast load model for SDOF method of one-way reinforced concrete slab," *EPJ Web of Conferences*, vol. 26, pp. 4–16, 2012.

[13] C. H. Dowding and C. Gilbert, "Dynamic stability of rock slopes and high frequency traveling waves," *Journal of Geotechnical Engineering*, vol. 114, no. 10, pp. 1069–1088, 1998.

[14] S. H. Zhang, L. S. Liu, and Q. L. Zhong, "Study on the energy distribution characteristics of blasting seismic wave in open slope," *Journal of Vibration and Shock*, vol. 38, no. 7, pp. 224–232, 2019.

[15] A. Kesimal, B. Ercikdi, and F. Cihangir, "Environmental impacts of blast-induced acceleration on slope instability at a limestone quarry," *Environmental Geology*, vol. 54, no. 2, pp. 381–389, 2008.

[16] Y. G. Hu, W. B. Lu, and M. Chen, "Comparison of blast-induced damage between presplit and smooth blasting of high rock slope," *Rock Mechanics and Rock Engineering*, vol. 47, no. 4, pp. 1307–1320, 2014.

[17] Y. Q. Ren, J. M. Zhang, and Y. Li, "Study into influence of blasting dynamic load on slope stability based on numerical simulation," *Journal of Natural Disasters*, vol. 22, no. 5, pp. 262–268, 2013.

[18] X. Z. Shi and S. R. Chen, "Delay time optimization in blasting operations for mitigating the vibration-effects on final pit walls' stability," *Soil Dynamics and Earthquake Engineering*, vol. 31, no. 8, pp. 1154–1158, 2011.

[19] G. G. U. Aldas and B. Ecevitoglu, "Waveform analysis in mitigation of blast-induced vibrations," *Journal of Applied Geophysics*, vol. 66, no. 1, pp. 25–30, 2008.

[20] D. P. Blair, "Some problems associated with standard charge weight vibration scaling laws," in *Proceedings of the 3rd International Symposium on Fragmentation by Blasting*, pp. 149–158, ISFB, Brisbane, Australia, February 1990.

[21] D. P. Blair, "Blast vibration control in the presence of delay scatter and random fluctuations between blastholes," *International Journal for Numerical and Analytical Methods in Geomechanics*, vol. 17, no. 2, pp. 95–118, 1993.

[22] D. P. Blair, "Statistical models for ground vibration and airblast," *Fragblast*, vol. 3, no. 4, pp. 335–364, 1999.

[23] D. P. Blair, "Non-linear superposition models of blast vibration," *International Journal of Rock Mechanics and Mining Sciences*, vol. 45, no. 2, pp. 235–247, 2008.

[24] S. H. Chen, J. Wu, and Z. H. Zhang, "Influence of millisecond time, charge length and detonation velocity on blasting vibration," *Journal of Central South University*, vol. 22, no. 12, pp. 4787–4796, 2015.

[25] X. M. Liu and S. H. Chen, "Surface vibration waveform prediction and effect analysis of group hole millisecond blasting," *Journal of Geotechnical Engineering*, vol. 42, no. 3, pp. 1–10, 2020.

[26] S. K. Mandal, "Mathematical model to locate interference of blast waves from multi-hole blasting rounds," *Journal of Mines, Metals and Fuels*, 2012.

[27] M. E. Kalinski, "Effect of vibroseis arrays on ground vibrations: a numerical study," *Journal of Environmental & Engineering Geophysics*, vol. 12, no. 3, pp. 281–287, 2007.

[28] R. S. Yang, C. X. Ding, and G. L. Yang, "Experimental study on explosion crack growth characteristics of millisecond blasting," *Vibration and Shock*, vol. 36, no. 24, pp. 97–102, 2017.

[29] C. L. Yang, G. W. Cao, and X. Z. Yang, "Uniform formula for the riemann solutions of a scalar combustion model," *Acta Mathematica Scientia*, vol. 36, no. 5, pp. 1405–1418, 2016.

[30] J. D. Schall, P. L. Thompson, and S. M. Zerges, *Hydraulic Design of Highway Culverts*, US Departement of transportation, USA, 2012.
[31] State Administration of Work Safety, *Coal Mine Safety Regulations*, Beijing Coal Industry Press, Beijing, China, 2016.
[32] X. K. Zou, *Study on Blasting Dynamic Response Characteristics and Damping Technology of Shallow Buried Multi-Arch Tunnel Excavation*, Southwest Jiao-tong University, Chengdu, China, 2016.
[33] Y. R. Zheng, "Development and application of numerical limit analysis method for rock and soil," *Journal of Rock Mechanics and Engineering*, vol. 31, no. 7, pp. 1297–1316, 2012.
[34] M. Chen, W. B. Lu, and L. Wu, "Study on safety threshold of blasting vibration velocity of high rock slope of Xiao-wan Hydropower Station," *Journal of Rock Mechanics and Engineering*, vol. 26, no. 1, pp. 51–56, 2012.
[35] R. Q. Huang, "Dynamic process and stability control of high rock slope development," *Journal of Rock Mechanics and Engineering*, vol. 27, no. 08, pp. 1525–1544, 2008.
[36] N. Jiang, C. B. Zhou, and W. Ping, "Elevation effect of blasting vibration velocity of rock slope," *Journal of Central South University*, vol. 45, no. 1, pp. 237–243, 2014.